

# Antiproton-nucleus collisions simulation within a kinetic approach with relativistic mean fields.

A.B. Larionov<sup>1,2\*</sup>, I.A. Pshenichnov<sup>1,3</sup>, I.N. Mishustin<sup>1,2</sup>, and W. Greiner<sup>1</sup>

<sup>1</sup>*Frankfurt Institute for Advanced Studies,*

*J.W. Goethe-Universität, D-60438 Frankfurt am Main, Germany*

<sup>2</sup>*Russian Research Center Kurchatov Institute, 123182 Moscow, Russia*

<sup>3</sup>*Institute for Nuclear Research, Russian Academy of Science, 117312 Moscow, Russia*

(Dated: November 11, 2018)

## Abstract

The Giessen Boltzmann-Uehling-Uhlenbeck transport model with relativistic mean fields is used to simulate  $\bar{p}$ -nucleus collisions. Antiproton absorption cross sections and momentum distributions of annihilation products are calculated by varying the  $\bar{p}$  coupling strength to the mean meson fields. Parameters of the antiproton-nucleus optical potential are extracted from the comparison of the model calculations with experimental data.

PACS numbers: 25.43.+t;21.30.Fe;24.10.-i

---

\* Corresponding author.

E-mail address: larionov@fias.uni-frankfurt.de

The real and imaginary parts of the antiproton optical potential are key quantities which determine  $\bar{p}$ -nucleus scattering at low [1, 2, 3] and intermediate [4] energies, as well as the existence of deeply bound  $\bar{N}$ -nucleus states [5, 6, 7, 8, 9, 10]. The  $\bar{p}N$  interaction in nuclear matter is, moreover, a challenging problem by itself, since it is subject to strong in-medium modifications. Indeed, in the simplest  $t\rho$ -approximation the real part of the  $\bar{p}$  optical potential is repulsive and about 100 MeV high for the  $\bar{N}N$  amplitude  $t$  taken at threshold [11], while  $\bar{p}$ -atomic phenomenology requires a strong attraction [9, 10, 11].

Usually the nuclear part of the  $\bar{p}$  optical potential is parameterized in a Woods-Saxon (WS) form

$$V_{\text{opt}} \simeq -\frac{V_0}{\exp\left(\frac{r-R_R}{a_R}\right) + 1} - \frac{iW_0}{\exp\left(\frac{r-R_I}{a_I}\right) + 1} . \quad (1)$$

In spite of several previous attempts to fix the  $\bar{p}$  optical potential, considerable ambiguity still remains in its parameters. The angular distributions of elastically scattered antiprotons favour a shallow real part  $V_0 = 0 \div 70$  MeV and a deep imaginary part  $W_0 = 70 \div 150$  MeV in the interior of a nucleus [1, 2, 3, 12, 13, 14, 15, 16]. The Glauber and optical model calculations for the  $\bar{p}$  absorption on nuclei [17, 18] also assume a negligibly small real part of  $V_{\text{opt}}$  and a strongly absorptive imaginary part. At the same time, the most recent combined analysis [9] of the X-ray transitions in antiprotonic atoms and of the radiochemical data has produced a deep real part  $V_0 = 110$  MeV and an imaginary part  $W_0 = 160$  MeV.

The  $\bar{p}$  optical potentials from elastic scattering and  $\bar{p}$ -atomic data are well determined only at the extreme periphery of a nucleus, corresponding to less than 10% of the central density [2, 9]. On the other hand,  $\bar{p}$  production in proton-nucleus and nucleus-nucleus collisions probes the  $\bar{p}$  potential deeply inside the nucleus and favours  $V_0 = 100 \div 200$  MeV consistent with a dispersion relation between real and imaginary parts of  $V_{\text{opt}}$  [19]. However, the microscopic transport analysis of Ref. [19] is also sensitive to rather uncertain in-medium elementary  $\bar{p}$ -production cross sections close to threshold.

The purpose of this work is to extract the information on a  $\bar{p}$  optical potential from the data on  $\bar{p}$  absorption cross section on nuclei [3, 4, 20, 21] and from the data on inclusive pion and proton production from low-energy  $\bar{p}$  annihilation in nuclei [22]. Here, the absorption means the removal of a  $\bar{p}$  from a beam caused by the annihilation, (in)elastic scattering and charge exchange reactions on individual nucleons. The diffractive elastic scattering on a nucleus as a whole is excluded from the absorption cross section. Since the absorption

requires at least one  $\bar{p}N$  collision, it is sensitive to the  $\bar{p}$  optical potential in a deeper region of a nucleus with respect to the case of diffractive elastic scattering. Indeed, the annihilation of 180 MeV antiprotons takes place at about half-density radius [23, 24]. By the same argument, the proton and pion production from  $\bar{p}$  annihilation on nuclei should also probe the  $\bar{p}$  optical potential at about half-density radius.

In our calculations, we have applied the Giessen Boltzmann-Uehling-Uhlenbeck (GiBUU) model [25]. This model solves a system of semiclassical kinetic equations for baryons, antibaryons and mesons coupled via collision terms and mean fields. The phase space distribution function of every particle species is projected on a set of point-like test particles. The coordinates  $\mathbf{r}_j$  and space components of the kinetic four-momentum  $p_j^{*\mu}$  of a baryon ( $j = B$ ) or an antibaryon ( $j = \bar{B}$ ) test particle are propagated in time according to the following Hamiltonian-like equations (c.f. [26, 27, 28] and refs. therein):

$$\dot{\mathbf{r}}_j = \frac{\mathbf{p}_j^*}{p_j^{*0}}, \quad (2)$$

$$\dot{p}_j^{*k} = \frac{p_{j\mu}^*}{p_j^{*0}} F_j^{k\mu} + \frac{m_j^*}{p_j^{*0}} \frac{\partial m_j^*}{\partial r_k} \quad (3)$$

with  $k = 1, 2, 3$  and  $\mu = 0, 1, 2, 3$ . The particles are assumed to be on the effective mass shell,  $p_j^{*0} = \sqrt{(\mathbf{p}_j^*)^2 + (m_j^*)^2}$ . The kinetic four-momentum is defined as  $p_j^{*\mu} \equiv p_j^\mu - V_j^\mu$ , where  $p_j^\mu$  is a canonical four-momentum and

$$V_j^\mu = g_{\omega j} \omega^\mu + g_{\rho j} \tau^3 \rho^{3\mu} + \frac{e}{2} (B_j + \tau^3) A^\mu \quad (4)$$

is a vector field with  $\tau^3 = +1$  for  $p$  and  $\bar{n}$ ,  $\tau^3 = -1$  for  $\bar{p}$  and  $n$ , and  $B_B = +1$ ,  $B_{\bar{B}} = -1$  being the baryon number. The field tensor in the r.h.s. of (3) is defined as  $F_j^{\nu\mu} \equiv \partial^\nu V_j^\mu - \partial^\mu V_j^\nu$ . The effective mass  $m_j^*$  is expressed in terms of a scalar potential  $S_j = g_{\sigma j} \sigma$  as  $m_j^* = m_j + S_j$ . Mesonic mean fields included into the model are  $(I, S) = (0, 1)$   $\omega$ ,  $(1, 1)$   $\boldsymbol{\rho}$ , and  $(0, 0)$   $\sigma$  with  $g_{\omega j}$ ,  $g_{\rho j}$ , and  $g_{\sigma j}$  being the respective coupling constants. The time component of the electromagnetic field, i.e. Coulomb potential, is also taken into account. The mesonic mean fields and Coulomb potential are calculated by solving the field equations with source terms provided by the currents and scalar density of test particles on the basis of a Relativistic Mean Field (RMF) model [26, 27, 28]. Initial positions and momenta of the test particles in the ground state nuclei are chosen randomly according to the spatial density distributions and the local Fermi momentum distribution. The proton and neutron densities are taken in a WS form consistent with a Skyrme Hartree-Fock systematics [29].

The RMF and optical models can be related via a Schrödinger equivalent potential [9, 30]:

$$\text{Re}(V_{\text{opt}}) = S_j + V_j^0 + \frac{S_j^2 - (V_j^0)^2}{2m_j} + \frac{V_j^0}{m_j} E_{\text{lab}}, \quad (5)$$

where  $E_{\text{lab}} = \sqrt{p_{\text{lab}}^2 + m_j^2} - m_j$  is the kinetic energy of a beam particle far away from a nucleus. The real part of the  $\bar{p}$  optical potential becomes deeper with increasing  $E_{\text{lab}}$  due to the negative vector potential, in distinction to the real part of the proton optical potential [30].

The  $\sigma$ -,  $\omega$ - and  $\rho$ -nucleon coupling constants have been taken from the NL3 model [31] providing a very good description of the ground states for both spherical and deformed nuclei. The meson-antinucleon coupling constants are quite uncertain. Following [8], we introduce  $g_{\omega\bar{N}} = -\xi g_{\omega N}$ ,  $g_{\rho\bar{N}} = \xi g_{\rho N}$ ,  $g_{\sigma\bar{N}} = \xi g_{\sigma N}$ , where  $0 < \xi \leq 1$  is an adjustable parameter. The case of  $\xi = 1$  corresponds to the  $G$ -parity transformed nucleon fields. For  $\xi = 1$ , neglecting the Coulomb field, the value of the  $\bar{p}$  vector potential in nuclear matter at the saturation density  $\rho_0 = 0.148 \text{ fm}^{-3}$  is  $V_{\bar{p}}^0 = -308 \text{ MeV}$ , while the scalar potential is  $S_{\bar{p}} = -380 \text{ MeV}$ . This gives an extremely deep real part,  $\text{Re}(V_{\text{opt}}) = -661 \text{ MeV}$ . Below, we will try to find out the values of  $\xi$  which are best suited to describe  $\bar{p}$  absorption and annihilation data on nuclei.

The antinucleon-nucleon collision terms in kinetic equations describe the elastic scattering, inelastic production and annihilation processes:  $\bar{N}N \rightarrow \bar{N}N$  (including charge exchange),  $\bar{N}N \rightarrow \bar{B}B + \text{mesons}$ ,  $\bar{N}N \rightarrow \text{mesons}$ . The cross sections of these processes are based on the experimental data parameterizations [32, 33]. The  $\bar{N}N$  annihilation has been described on the basis of a statistical model [34, 35]. The annihilation final state includes up to six particles, which are various combinations of  $\pi$ ,  $\eta$ ,  $\omega$  and  $\rho$  mesons. The annihilation model was originally used in Ref. [34] for slow antiprotons, but after the proper parameter adjustment the model also describes successfully pion spectra and multiplicity distributions in  $\bar{p}p$  annihilation in flight, up to  $p_{\text{lab}} \simeq 10 \text{ GeV}/c$  [35]. A more detailed description of the  $\bar{N}N$  collision channels implementation in the GiBUU model will be given elsewhere.

To calculate collision terms, we have used a full ensemble technique of the test particle method (c.f. [36] and refs. therein). The full ensemble technique, in distinction to the cascade-like parallel ensemble one, solves the Boltzmann equation more precisely as the binary collisions are better localized. In the  $\bar{p}$  absorption calculation on nuclei, we have turned off the two-body collisions of the secondary particles in order to enforce a Glauber-

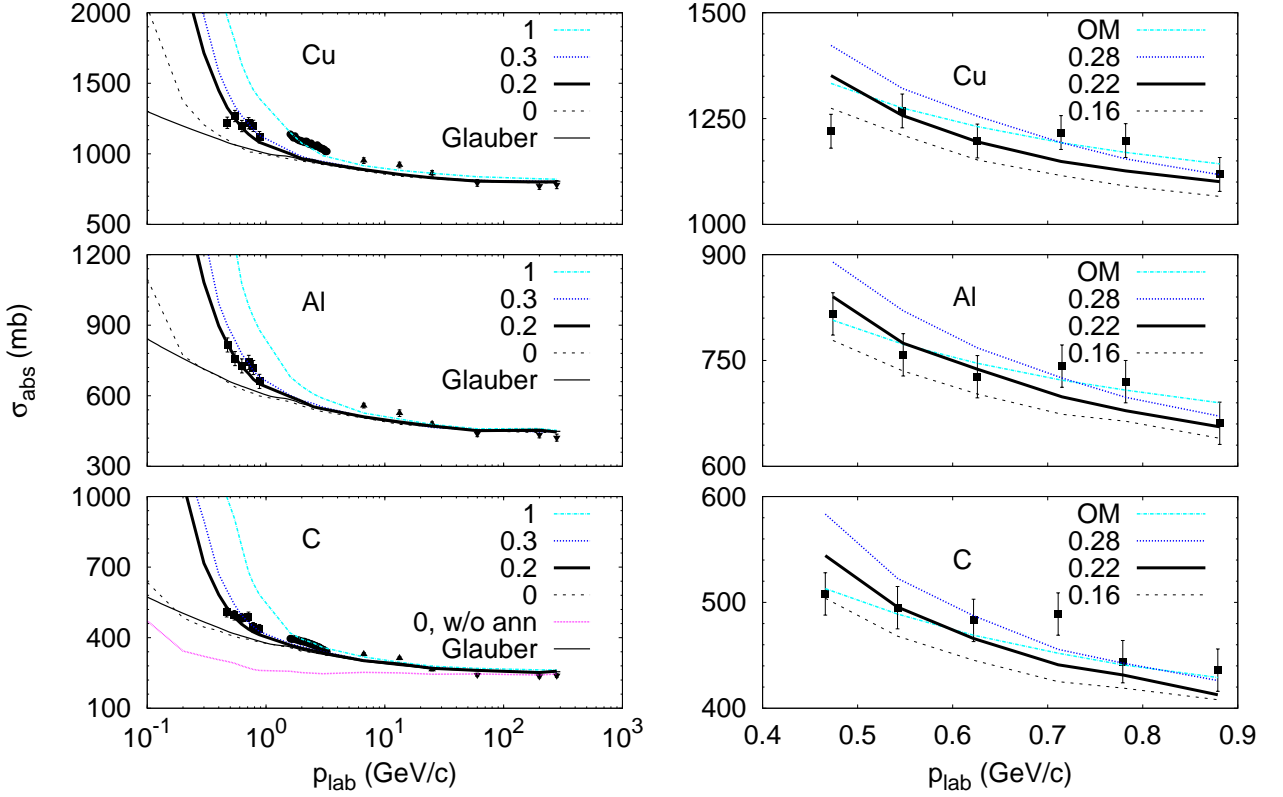


FIG. 1: (Color online)  $\bar{p}$  absorption cross section on various nuclei vs the beam momentum. The lines marked with the value of a scaling factor  $\xi$  show the GiBUU results. On the left three panels, thin solid lines represent the Glauber model calculation, Eq.(7). For the  $\bar{p}+^{12}\text{C}$  system, a calculation with  $\xi = 0$  without annihilation is additionally shown by the dotted line on the lower left panel. Data are from Ref. [3] (filled boxes), Ref. [4] (filled circles), Ref. [20] (filled triangles) and Ref. [21] (filled upside-down triangles). The right three panels show  $\sigma_{\text{abs}}$  at lower beam momenta, where the actual fit has been done. The optical model (OM) results are from Ref. [3].

type description.

Fig. 1 shows the  $\bar{p}$  absorption cross section on  $^{12}\text{C}$ ,  $^{27}\text{Al}$  and  $^{64}\text{Cu}$  as a function of the

beam momentum. The absorption cross section has been computed as

$$\sigma_{\text{abs}} = 2\pi \int_0^{b_{\text{max}}} db b P_{\text{abs}}(b) , \quad (6)$$

where  $b$  is an impact parameter and  $P_{\text{abs}}(b)$  is the probability of the  $\bar{p}$  absorption, i.e. suffering at least one (in)elastic scattering or annihilation on a nucleon. The maximum value of the impact parameter,  $b_{\text{max}} \simeq (1.1A^{1/3} + 5)$  fm, has been chosen large enough to have  $P_{\text{abs}}(b_{\text{max}}) = 0$  in a GiBUU calculation. Without any mean field effects, Eq.(6) can be reduced to a simple Glauber formula [4, 37]

$$\sigma_{\text{abs}}^{\text{Glauber}} = 2\pi \int_0^{\infty} db b [1 - \exp(-\bar{\sigma}_{\text{tot}} S(b))] , \quad (7)$$

where  $\bar{\sigma}_{\text{tot}}$  is the isospin-averaged total  $\bar{p}N$  cross section and

$$S(b) = 2 \int_0^{\infty} \rho(\sqrt{b^2 + s^2}) ds \quad (8)$$

is the nuclear density integral along the straight line trajectory of a projectile with  $\rho(r)$  being the nuclear density at the radial distance  $r$ . The Glauber formula (7) describes quite well the experimental absorption cross section at very high beam momenta. However, there are significant deviations of Eq. (7) from the data at  $p_{\text{lab}} \leq 20$  GeV/c.

At  $p_{\text{lab}} > 0.4$  GeV/c, the GiBUU calculations with  $\xi = 0$  are very close to the Glauber model, as expected. At smaller beam momenta, the attractive Coulomb potential increases the absorption cross section with respect to Eq. (7). As one can see from Fig. 1, the agreement with the data can only be achieved when the mean meson fields are introduced. This can be understood as follows: In the calculation without any mean field, the beam particles with impact parameters larger than the nuclear radius do not experience binary collisions since they propagate along straight-line trajectories. Turning on the attractive mean field bends trajectories of the beam particles toward the nucleus. Thus, the attractive mean field makes a larger part of the beam flux to experience two-body collisions.

The sensitivity of the absorption cross section to the  $\bar{p}$  mean field grows with decreasing beam momentum. Thus we have selected the KEK data [3] at  $p_{\text{lab}} = 470 \div 880$  MeV/c to find the optimum value of the parameter  $\xi$  for  $^{12}\text{C}$ ,  $^{27}\text{Al}$  and  $^{64}\text{Cu}$  targets. As one can see from Fig. 1,  $\xi = 0.2 \div 0.3$  provides the best overall agreement with the data. A stronger attraction, i.e. larger  $\xi$ , leads to an overestimation of the absorption cross section at  $p_{\text{lab}} < 1$

TABLE I: The scaling factor  $\xi$  of the antibaryon coupling constants and  $\bar{p}$  optical potential parameters  $V_0$  (MeV),  $R_R$  (fm),  $a_R$  (fm),  $W_0$  (MeV),  $R_I$  (fm),  $a_I$  (fm) (see Eq. (1)), obtained by fitting the data of Ref. [3] for different nuclei. The  $\chi^2$  values per degree of freedom ( $F = 5$ ) and the standard errors of the scaling factor  $\xi$  are given. The errors of the real depth  $V_0$  are caused by a variation of  $\xi$  by one standard error. The errors of all other parameters are less than 2% and are not shown.

Nucleus	$\xi$	$\chi^2/F$	$V_0$	$R_R A^{-1/3}$	$a_R$	$W_0$	$R_I A^{-1/3}$	$a_I$
$^{12}\text{C}$	$0.22 \pm 0.03$	2.2	$153 \pm 21$	1.00	0.63	110	0.97	0.52
$^{27}\text{Al}$	$0.21 \pm 0.04$	1.1	$162 \pm 37$	1.04	0.64	108	0.99	0.66
$^{64}\text{Cu}$	$0.21 \pm 0.04$	3.3	$153 \pm 29$	1.09	0.64	103	1.06	0.65

GeV/c. Minimizing  $\chi^2$  deviation from six data points for each nucleus results in  $\xi$  values listed in Table I. The global fit to eighteen data points for all three nuclei produces the scaling factor  $\xi = 0.21 \pm 0.03$  with  $\chi^2/F = 2.0$  ( $F = 17$ ).

The quality of our calculations is visualised in Fig. 1 (right panels), where we also show for a comparison the absorption cross sections from the optical model calculations of Ref. [3]. Our absorption cross section drops with increasing beam momentum somewhat faster than the data do. The optical model describes the data slightly better. However, the optical potential of Ref. [3] has the two free parameters,  $V_0$  and  $W_0$ , vs only one, i.e.  $\xi$  (or, equivalently,  $V_0$ ) in our model. Moreover, the fixed geometrical parameters of the optical potential of Ref. [3] are rather arbitrary and, therefore, can be considered as free parameters too.

We have also extracted the parameters of a  $\bar{p}$  optical potential for the best fit values of  $\xi$ . The real part of  $V_{\text{opt}}$  has been determined from Eq. (5) dropping the Coulomb field contribution in  $V_{\bar{p}}^0$ . The imaginary part has been calculated as

$$\text{Im}(V_{\text{opt}}) = -\frac{1}{2} \langle v_{\text{rel}} \sigma_{\text{tot}}^{\text{med}} \rangle \rho, \quad (9)$$

where the averaging is done with respect to the Fermi momenta of nucleons,  $v_{\text{rel}}$  is the relative velocity of an incoming  $\bar{p}$  and a nucleon,  $\sigma_{\text{tot}}^{\text{med}}$  is the total in-medium  $\bar{p}N$  cross section computed taking into account the Pauli blocking of a final nucleon state for the (in)elastic scattering contribution, and  $\rho$  is the density of nucleons. The radial dependencies

of the real and imaginary parts, Eqs. (5) and(9), have been approximated by Eq. (1) for  $E_{\text{lab}} = 0$ . Resulting WS parameters are listed in Table I. The mass dependence of the WS radii  $R_R$ ,  $R_I$  appreciably deviates from a standard  $\propto A^{1/3}$  behaviour, which is mostly caused by the underlying realistic neutron and proton density distributions from a Skyrme Hartree-Fock systematics [29]. The extraction of the optical potential parameters is far from unique. In particular, the WS depths are sensitive to the assumed size parameters, and there is no guarantee that the WS optical potential parameters listed in Table I result in as good fit to the data as provided by the GiBUU calculation.

One could also notice from Fig. 1 (left panels), that the BNL [4] and Serpukhov [20] data at  $p_{\text{lab}} = 1.6 \div 20$  GeV/c are consistent with  $\xi = 1$ , i.e. with the G-parity value of the real part of  $\bar{p}$  optical potential. A similar result based on the data [4] has been obtained earlier in Ref. [30]. The G-parity motivated  $\bar{p}$  potential is, however, not supported by more recent low energy data of Ref. [3]. It would be, therefore, quite useful to perform the new measurements of  $\bar{p}$  absorption cross sections above 1 GeV/c, which is accessible at the future Facility for Antiproton and Ion Research (FAIR).

As shown in Fig. 2, further constraints on the  $\bar{p}$  optical potential can be obtained from inclusive momentum spectra of positive pions and protons produced in  $\bar{p}+^{12}\text{C}$  and  $\bar{p}+^{238}\text{U}$  interactions at 608 MeV/c. The two-slope structure of the pion spectra with the slope change at  $p \simeq 0.3$  GeV/c is caused by pion-nucleon rescattering mediated by the  $\Delta(1232)$  resonance. Higher momentum pions leave the nucleus practically without interactions with nucleons. Lower momentum pions are either absorbed via  $\Delta(1232)$  resonances,  $\Delta N \rightarrow NN$ , or get decelerated in collisions with nucleons.

The calculated proton spectra also change their slopes at  $p \simeq p_F$ , where  $p_F = 0.27$  GeV/c is the Fermi momentum of nucleons. High momentum protons are knocked-out from a nucleus by energetic pions. The lower part of a proton momentum spectrum is populated by the slow evaporated protons produced after the fast cascading pions and nucleons have already left the nucleus.

Varying parameters of the antiproton mean field influences the momentum spectra of annihilation products only moderately. The attraction of incoming  $\bar{p}$  to a nucleus increases the annihilation probability. On the other hand, the invariant energy of an annihilating  $\bar{p}N$  pair is reduced by a stronger  $\bar{p}$ -attraction. As a consequence, the multiplicities and kinetic energies of annihilation mesons get reduced. A partial cancellation of these two effects leads



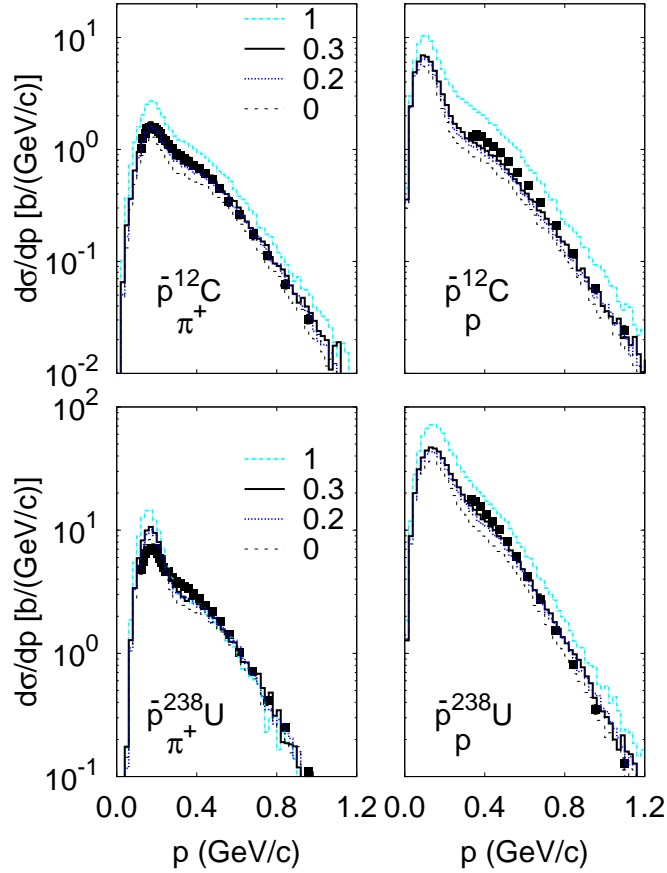


FIG. 2: (Color online) The angle-integrated  $\pi^+$  and proton laboratory momentum inclusive spectra from  $\bar{p}$  interaction with  $^{12}\text{C}$  and  $^{238}\text{U}$  at 608 MeV/c. Calculated histograms are denoted by the value of the scaling factor  $\xi$ . Data are from [22].

to a rather weak sensitivity of the momentum spectra to the  $\bar{p}$  mean field. Overall, the calculation with  $\xi = 0.3$  is in the best agreement with  $\pi^+$  and proton momentum spectra at 608 MeV/c.

In conclusion, we have applied the hadron transport GiBUU model to describe  $\bar{p}$ -nucleus interactions at the beam momenta in the range  $0.4 \div 280$  GeV/c. The depth of the real part of the  $\bar{p}$  optical potential, extracted by fitting the KEK data [3] at low beam momenta is  $V_0 \simeq 150 \pm 30$  MeV which is about 40% deeper than the value reported by Friedman et al [9]. However, depths corresponding to different geometries – size parameters – may not be

directly comparable with each other.

The annihilation spectra of positive pions and protons measured at LEAR [22] favour even deeper real part,  $V_0 \simeq 220 \pm 70$  MeV. Such attractive potentials may lead to the cold compression effect when  $\bar{p}$  penetrates deeply into the nuclear interior [7, 8, 27, 38]. This possibility deserves further studies in view of future FAIR experiments with antiproton beams.

### Acknowledgments

The support by the Frankfurt Center for Scientific Computing is gratefully acknowledged. We thank O. Buss, M. Kaskulov and L.M. Satarov for stimulating discussions. We are also indebted to T. Gaitanos for his permission to use the RMF implementation of the  $\rho$ -meson and Coulomb fields in the GiBUU model before publication. We are grateful to the referee for the productive exchange of ideas leading to the modified discussion. This work was (financially) supported by the Helmholtz International Center for FAIR within the framework of the LOEWE program (Landesoffensive zur Entwicklung Wissenschaftlich-Ökonomischer Exzellenz) launched by the State of Hesse, by the DFG Grant 436 RUS 113/957/0-1 (Germany), and by the Grants NS-3004.2008.2 and RFBR-09-02-91331 (Russia).

- 
- [1] D. Garreta et al., Phys. Lett. **B135**, 266 (1984).
  - [2] D. Garreta et al., Phys. Lett. **B149**, 64 (1984).
  - [3] K. Nakamura et al., Phys. Rev. Lett. **52**, 731 (1984).
  - [4] R. J. Abrams et al., Phys. Rev. **D4**, 3235 (1971).
  - [5] C. Y. Wong, A. K. Kerman, G. R. Satchler, and A. D. Mackellar, Phys. Rev. **C29**, 574 (1984).
  - [6] A. J. Baltz, C. B. Dover, M. E. Sainio, A. Gal, and G. Toker, Phys. Rev. **C32**, 1272 (1985).
  - [7] T. Buervenich et al., Phys. Lett. **B542**, 261 (2002).
  - [8] I. N. Mishustin, L. M. Satarov, T. J. Buervenich, H. Stoecker, and W. Greiner, Phys. Rev. **C71**, 035201 (2005).
  - [9] E. Friedman, A. Gal, and J. Mares, Nucl. Phys. **A761**, 283 (2005).
  - [10] E. Friedman and A. Gal, Phys. Rept. **452**, 89 (2007).

- [11] C. J. Batty, E. Friedman, and A. Gal, Phys. Rept. **287**, 385 (1997).
- [12] C. J. Batty, E. Friedman, and J. Lichtenstadt, Phys. Lett. **B142**, 241 (1984).
- [13] J. Kronenfeld, A. Gal, and J. M. Eisenberg, Nucl. Phys. **A430**, 525 (1984).
- [14] C. J. Batty, E. Friedman, and J. Lichtenstadt, Nucl. Phys. **A436**, 621 (1985).
- [15] O. D. Dalkarov and V. A. Karmanov, Nucl. Phys. **A445**, 579 (1985).
- [16] E. Friedman and J. Lichtenstadt, Nucl. Phys. **A455**, 573 (1986).
- [17] L. A. Kondratyuk and M. G. Sapozhnikov, Sov. J. Nucl. Phys. **46**, 56 (1987).
- [18] H. Lenske and P. Kienle, Phys. Lett. **B647**, 82 (2007).
- [19] S. Teis, W. Cassing, T. Maruyama, and U. Mosel, Phys. Rev. **C50**, 388 (1994).
- [20] S. P. Denisov et al., Nucl. Phys. **B61**, 62 (1973).
- [21] A. S. Carroll et al., Phys. Lett. **B80**, 319 (1979).
- [22] P. L. McGaughey et al., Phys. Rev. Lett. **56**, 2156 (1986).
- [23] M. R. Clover, R. M. DeVries, N. J. DiGiacomo, and Y. Yariv, Phys. Rev. **C26**, 2138 (1982).
- [24] J. Cugnon and J. Vandermeulen, Nucl. Phys. **A445**, 717 (1985).
- [25] URL <http://gibuu.physik.uni-giessen.de/GiBUU>.
- [26] A. B. Larionov, O. Buss, K. Gallmeister, and U. Mosel, Phys. Rev. **C76**, 044909 (2007).
- [27] A. B. Larionov, I. N. Mishustin, L. M. Satarov, and W. Greiner, Phys. Rev. **C78**, 014604 (2008).
- [28] T. Gaitanos, H. Lenske, and U. Mosel, Phys. Lett. **B663**, 197 (2008).
- [29] H. Lenske, private communication.
- [30] A. Bouyssy and S. Marcos, Phys. Lett. **B114**, 397 (1982).
- [31] G. A. Lalazissis, J. Konig, and P. Ring, Phys. Rev. **C55**, 540 (1997).
- [32] J. Cugnon and J. Vandermeulen, Ann. Phys. (France) **14**, 49 (1989).
- [33] L. Montanet et al. (Particle Data Group), Phys. Rev. **D50**, 1173 (1994).
- [34] E. S. Golubeva, A. S. Iljinov, B. V. Krippa, and I. A. Pshenichnov, Nucl. Phys. **A537**, 393 (1992).
- [35] I. A. Pshenichnov, doctoral thesis, INR, Moscow, 1998.
- [36] O. Buss, L. Alvarez-Ruso, A. B. Larionov, and U. Mosel, Phys. Rev. **C74**, 044610 (2006).
- [37] R. J. Glauber and G. Matthiae, Nucl. Phys. **B21**, 135 (1970).
- [38] I. N. Mishustin and A. B. Larionov (2008), 0810.4030.

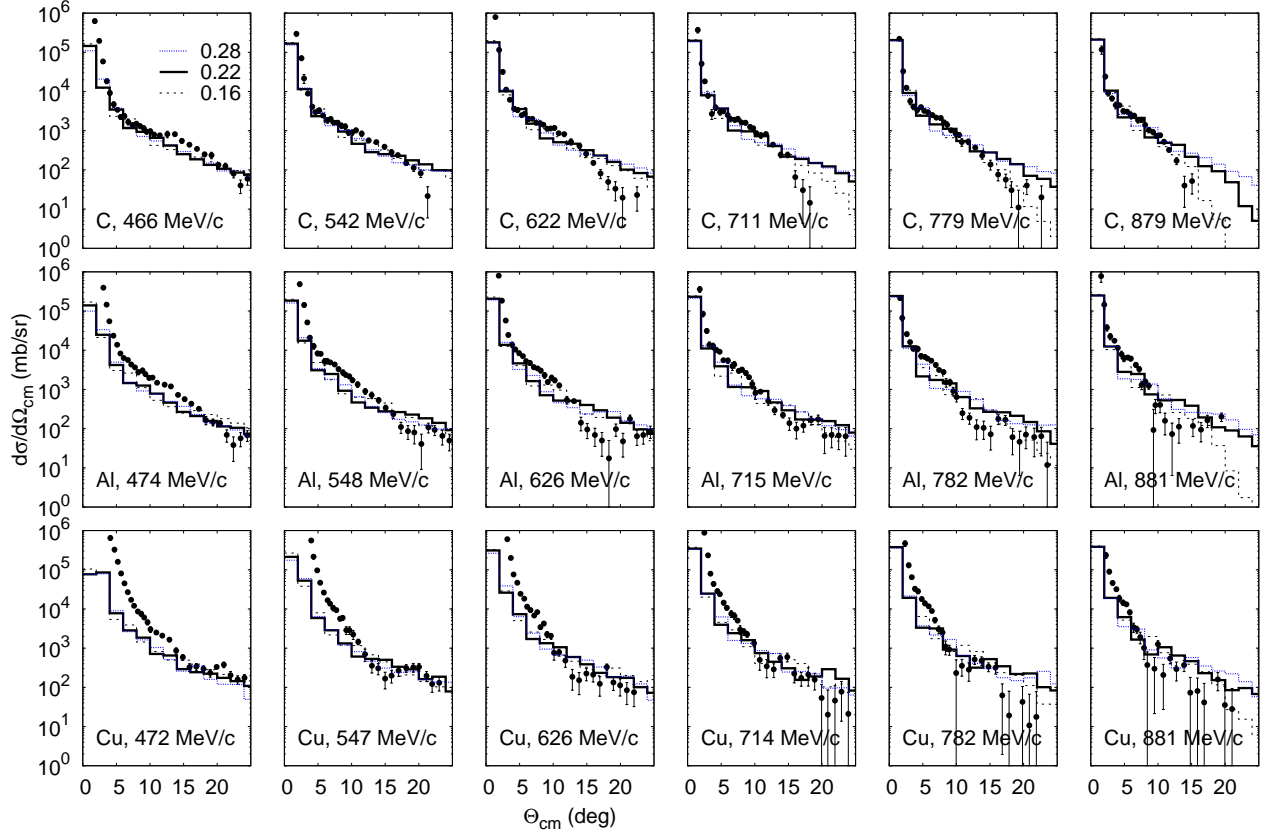


FIG. 3: (addition to the PRC version of the paper)  $\bar{p}$  differential elastic scattering cross section. The computed histograms are marked with the value of a scaling factor  $\xi$ . Data are from Ref. [3]. With some reservations for the semiclassical nature of our model, the agreement with the data is fairly good within the values of the scaling factor  $\xi = 0.22 \pm 0.06$ , except for small-angle scattering at lower beam momenta, where we underpredict the experiment rather substantially. This deficiency is, most probably, due to neglecting the Coulomb corrections on the distant parts of the  $\bar{p}$  trajectory (more than  $\simeq (1.1A^{1/3} + 5)$  fm from the nuclear centre). The detailed study of elastic scattering goes, however, beyond the scope of the present work.

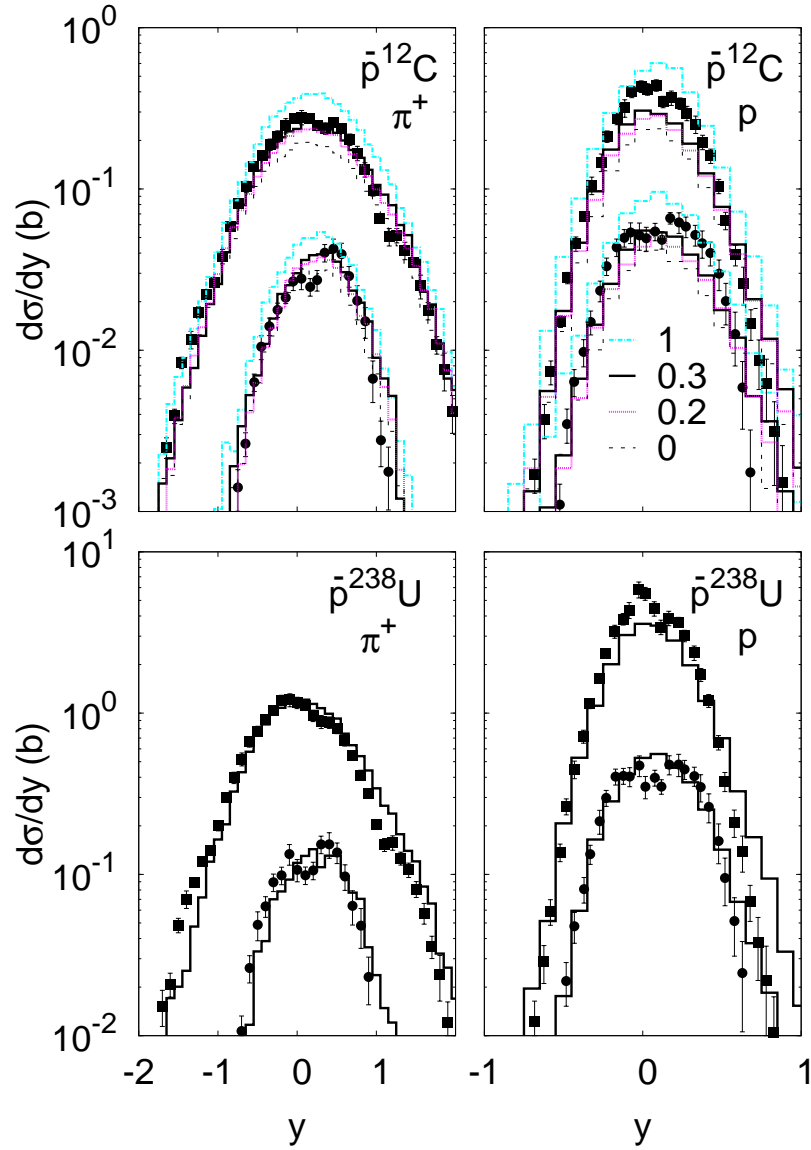


FIG. 4: (addition to the PRC version of the paper)  $\pi^+$  and proton laboratory rapidity spectra from antiproton interaction with  $^{12}\text{C}$  and  $^{238}\text{U}$  at 608 MeV/c. Calculated histograms are denoted by the value of the scaling factor  $\xi$ . For the  $\pi^+$  (proton) spectra, the upper lines and data points correspond to the transverse momenta  $p_T \geq 120$  (330) MeV/c, while lower lines and data points are computed for  $p_T \geq 500$  (600) MeV/c. Experimental data are from [22].